ENHANCED HIGH-TEMPERATURE MECHANICAL BEHAVIOR OF AN IN SITU TiAl MATRIX COMPOSITE REINFORCED WITH ALUMINA

D. Pilone ⓘ, A. Mondal, A. Brotzu and F. Felli
Department of ICMA, Sapienza University of Rome, Via Eudossiana 18, 00184 Roma, Italy

G. Pulci, L. Paglia and F. Marra
Department of ICMA, Sapienza University of Rome, INSTM Reference Laboratory for Engineering of Surface Treatments, Via Eudossiana 18, 00184 Rome, Italy

Abstract

A Ti-45Al-3Cr-2.5Nb alloy reinforced with in situ formed alumina has been produced by means of centrifugal casting by adding zirconium oxide in the crucible. The dispersion-strengthened alloy has been characterized to verify its microstructure and particle distribution. Mechanical tests carried out over the temperature range 850–950 °C highlighted that in situ formed alumina allows to increase the alloy yield stress by 21% at 850 °C and by 35% at 900 °C. Moreover, the in situ formed oxide particles produced an increase of the Young's modulus of about 10% at 850 °C and of about 8% at 900 °C. Considering that the tested alloy has a density that is about a half of nickel superalloys, obtaining high specific mechanical properties over the temperature range 850–950 °C can boost its application in the production of turbine blades.

Graphical abstract
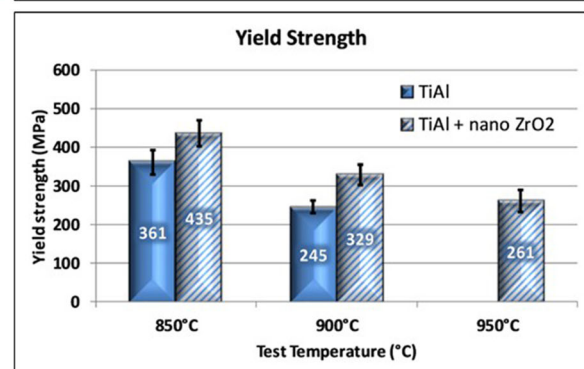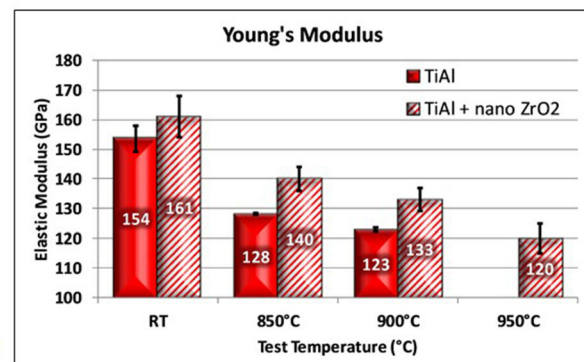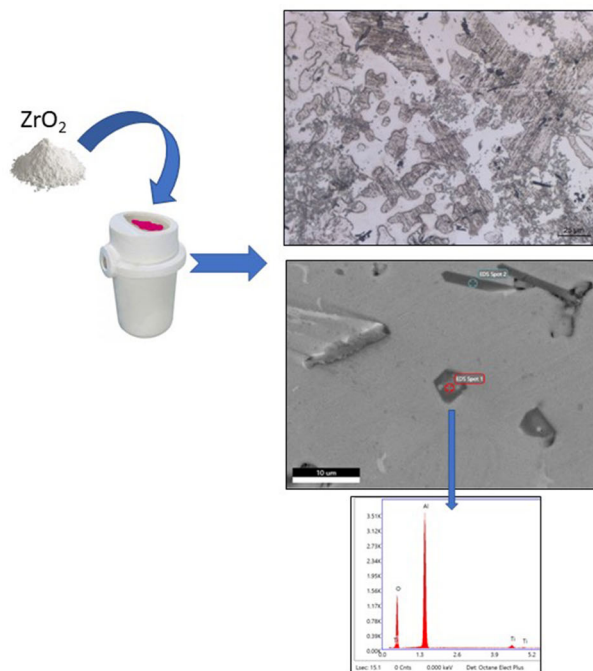
Introduction

In the last 20 years, titanium aluminides have become one of the most important high-temperature alloys to be researched due to their unique combination of mechanical properties, especially at elevated temperature, some of which are even superior to those of superalloys.[1–3] These alloys are generally used in aerospace[4,5] and automotive[6–9] sectors due to their low density (3.9–4.2 g/cm^3), high specific yield strength, high specific stiffness, good oxidation at high temperature and good creep properties.

In particular, γ-TiAl alloys are of uttermost importance. At elevated temperatures, especially above 600 °C, γ-TiAl alloys are superior, in terms of specific strength, to the heavier Ni-based superalloys.[1] Because of this, γ-TiAl alloys have become the leading material choice to replace Ni-based superalloys in gas turbine engines with an expected weight reduction of about 30–40%.[4] Over the past few decades, the research on TiAl was dedicated to the development and optimization of γ-TiAl-based alloys. Structurally, among the various phases, only α_2 (Ti$_3$Al) phase with a hexagonal D0$_{19}$ structure and γ(TiAl) phase with a tetragonal L1$_0$ structure were found to be the most suitable for structural materials.[10] Although γ-TiAl has a lot of advantageous properties, its ductility and fracture toughness are very low due to its long-range order.

Over the last few years, our team of researchers has been experimenting and studying ways to increase the ductility and toughness at low temperature of these alloys. The literature based on previous research on this alloy shows that γ-TiAl alloys, having a duplex structure, have allowable ductility at room temperature and low creep resistance at high temperature. It has been found that if the microstructure is fully lamellar, then the alloy shows excellent creep resistance but low room-temperature ductility. If the alloy is characterized by a mixture of lamellar colonies and γ grains, then the resulting alloy is an interesting structural material having mechanical properties that are sensitive to microstructure, grain size and micro-alloying. Many efforts have also been devoted to improve mechanical properties of TiAl-based alloys by controlling the lamellar orientation by the seeding technology[11] Studies and simulations have been carried out to limit residual stresses, which are very critical for these alloys, and to avoid the formation of defects such as shrinkage cavities.[12,13] Computer simulation modeling and experimental tests allowed to study the effect of cooling rates and temperature gradients on the formation of macroshrinkage porosity. Optimization of the alloy microstructure has been studied by several authors, and a novel apparatus that provides accurate control of mold pre-heating, pouring and alloy heat treatment with different cooling rates has been designed and tested with interesting results providing new insights into the production of TiAl intermetallic components.[14]

By analyzing the available literature, it can be seen that components made of this alloy are produced using hot isostatic pressing of powders, casting, additive manufacturing, with several processes already being used in the industry. Our research team has worked, over the years, on the development and characterization of TiAl alloys produced by centrifugal casting for use at high temperatures.[15–17] Most recently, the focus has been on the methods that allow to increase mechanical strength, Young's modulus and creep resistance. Dispersion strengthening of the metal matrix has been studied by adding particles characterized by high thermal stability and elastic modulus, such as oxides (Al$_2$O$_3$, Y$_2$O$_3$, CeO$_2$, ZrO$_2$ and ThO$_2$) and carbides (SiC, NbC, MoC, WC).[18]

Dispersion strengthening is a widespread practice in the industry, and it is extensively used to reinforce materials from steel to superalloys. This process is already being used to harden nickel-based superalloys used for aerospace engines[19] above 1000 °C.

In previous works related to this research, TiAl was dispersion-strengthened using nanometric Al$_2$O$_3$.[16] While the focus was on enhancing the mechanical properties of the alloy, microstructural investigation was also performed to study microstructure and dispersion homogeneity. A lot of research has been done in order to strengthen TiAl by in situ or ex situ methods, but all of them are focused on powder metallurgy or additive manufacturing.[20–23] In previous literature research, the in situ formation of alumina was explored with its beneficial effects on the mechanical properties and microstructure of the alloy by adding oxides such as Cr$_2$O$_3$ and Fe$_2$O$_3$.[24,25] But this research was based on hot isostatic pressing and mechanical properties were evaluated only at room temperature.

Aim of this research is the production and characterization of an in situ dispersion-strengthened TiAl alloy obtained by investment casting. This alloy has been studied and characterized by performing mechanical tests at various temperatures: from room temperature up to 950 °C.

Experimental Procedure

Investment casting was used to produce the specimens for mechanical testing. A wax pattern was prepared assembling different parts corresponding to the final cast. The pattern was constituted of 5 columns of size 4.5 mm × 4.5 mm × 55 mm. These columns were mounted on a conical runner to improve metal flow (Figure 1).

Once the wax pattern was created, a spinel-based refractory ceramic material was selected to avoid the metal-mold reaction.[26,27] For making the final mold, a cylindrical tube was filled with the ceramic slurry containing the wax pattern in the center of the tube. This was left to air-dry and solidify at room temperature for 24 h. Once dried, the wax pattern was melted by heating the mold in an oven at 150 °C for 2 h. The mold was then treated in a furnace following the following thermal cycle:

(1) Heating the mold up to 250 °C and staying at this temperature for 30 minutes.
(2) Heating the mold to 900 °C and staying at this temperature for 30 minutes.
(3) Cooling the mold up to 450 °C inside the furnace and staying at this temperature until casting.

A total of three castings were made with five specimens for each casting. Pure Ti, Al, Cr, and Nb were used for the casting. The alloying elements were melted in an induction furnace working under vacuum after six washing cycles with argon. Nanometric ZrO_2 (3% vol.) was added to the alloy. After induction melting, the molten metal was directly cast using centrifugal casting into the rotating mold. The mold with the molten metal was again kept in a furnace at 450 °C for 3 h in order to relieve the residual stresses. Once the metal was solidified and cooled to room temperature, the mold was broken, and the casting was extracted. The casting was then cut using a diamond-coated cutting blade to obtain the specimens.

The cut specimens were still not ready for mechanical tests because they had an irregular surface, and their dimensions were not the ones required for the mechanical tests. So the specimens were ground to obtain 2 mm × 4 mm × 45 mm specimens. This was done using SiC papers ranging from 80 to 240 grits. The samples were.[28,29] For the flexural bending test, a Zwick-Roell Z 2.5 testing machine (Zwick GmbH, Ulm, Germany) equipped with a Maytec furnace (up to 1600 °C), a 3-point-contact extensometer and a silicon carbide fully articulated flexural device (Maytech GmbH, Singen, Germany) was used. The samples were heated at 15 °C/min up to the final temperature, maintained at this temperature for 30 minutes and then subjected to high-temperature flexural tests, carried out at a constant crosshead speed of 0.5 mm/min. This value is suggested by the ASTM standards in order to minimize the test time and creep influence. The test duration varied accordingly depending on the test temperature and maximum deformation reached during the test, which corresponded to the standard recommendations. The elaboration of stress–strain curves allowed the evaluation of Young's modulus and yield stress. The strain measurement was taken by a properly designed displacement transducer using three alumina rods pushing against the tension face of the sample. The measurement of the sample deflection on the three separated points allowed to exclude the undesired contribution of thermal expansion of alumina extensometer rods. The experimental setup enables a direct and reliable measurement of the curvature of the sample, with appreciable improvements compared to the evaluation of crosshead travel or the direct measurement of the deflection of the central section of the sample. Young's modulus calculations were carried out using a regression of stress–strain curves between 40 and 80 MPa.

Some of the samples from different castings were ground and polished in order to perform microstructural examination, which was performed using an optical microscope and an electron microscope. The optical microscope used was Leica DMI 5000 (Leica, Wetzlar, Germany), while the scanning electron microscope was Tescan Mira3 (Kohoutovice, Czech Republic). A study was also performed to analyze the dispersoid distribution in the metal matrix. Samples were analyzed by energy dispersion spectroscopy (EDS) to verify chemical composition and fracture surfaces were inspected by SEM after the bending test using Hitachi S-2500 (Krefeld, Germany).

Results and Discussion

All castings had the same nominal composition, but there were slight compositional differences after the final casting. After the specimens were prepared, an EDS analysis was performed to obtain an average composition of the cast alloys. This is shown in Table 1.

After the alloy was poured, the microstructure of all the castings was analyzed after etching with Keller's reagent

Figure 1. Drawing of the wax pattern used to produce the specimens.

Table 1. Mean Composition of the Cast Alloy

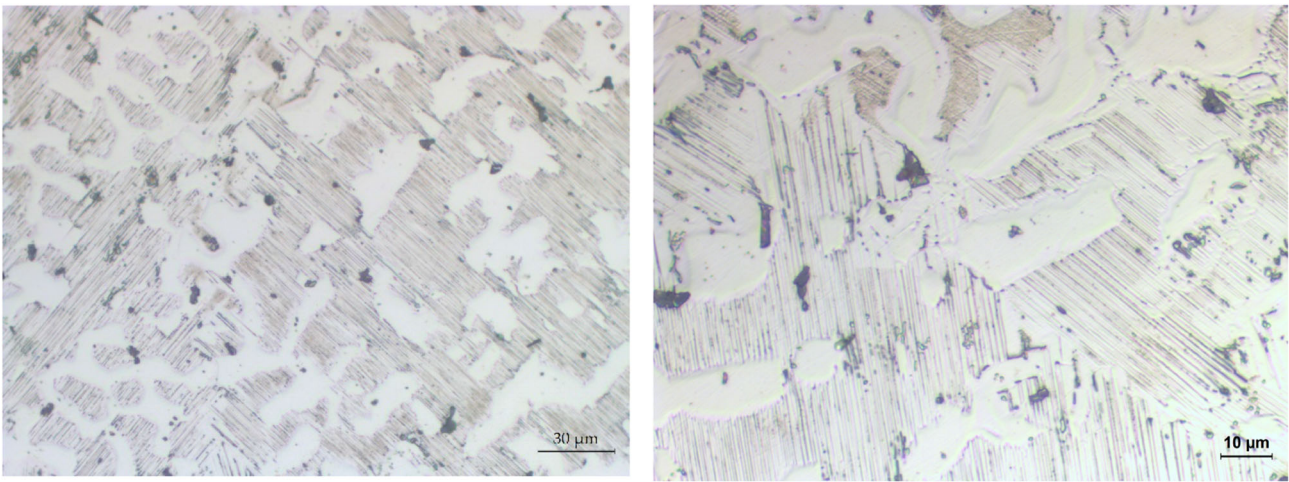| Elements	Aluminum	Titanium	Chromium	Niobium
Atomic%	45.11	49.33	3.05	2.51

Figure 2. Optical micrographs showing the microstructure of the cast alloy at two different magnifications.
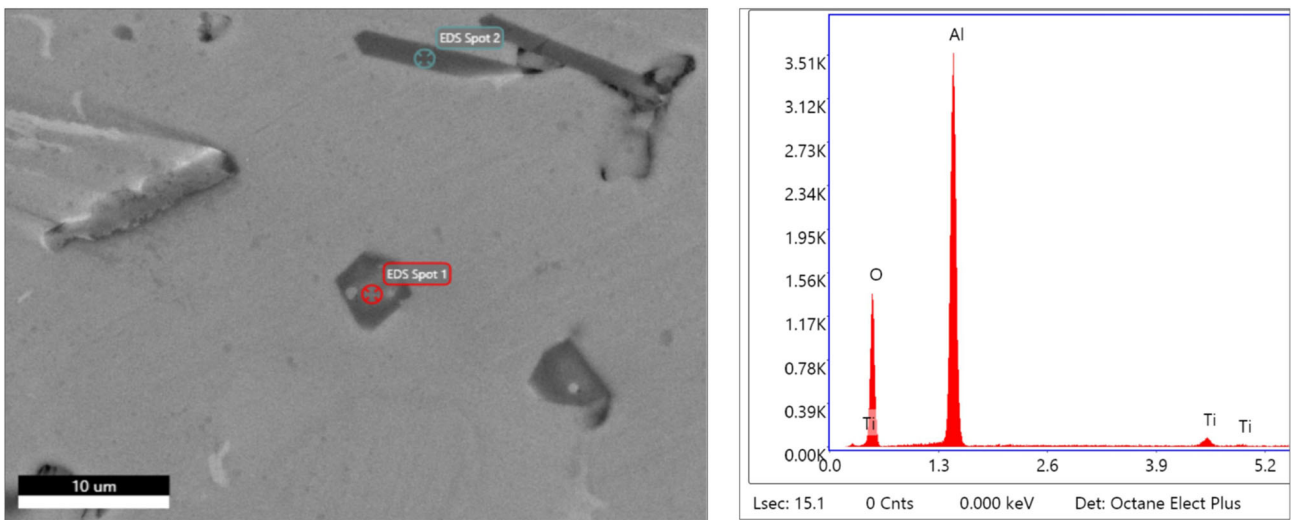

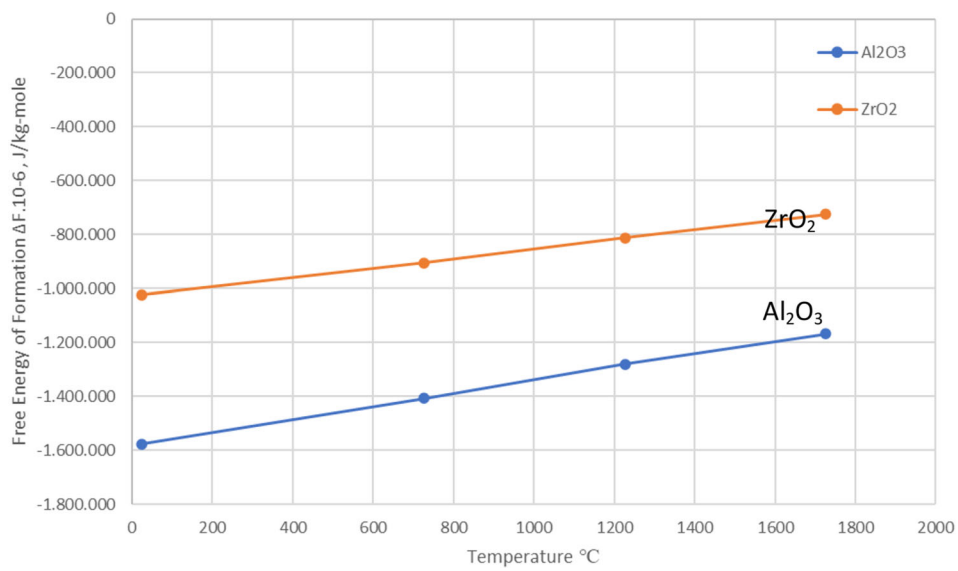**Figure 3. SEM image of the particles dispersed in the alloy and EDS spectrum showing their composition.**

Figure 4. Ellingham diagram.[30]

for 15 sec. Upon observation under the optical microscope, the microstructure consists mainly of γ grains and lamellar colonies of α_2 and γ phases (Figure 2). There was also the presence of black particles (circular, long flakes and polygonal in shape) and a small amount of an unidentified phase.

In order to examine these small phases and the black particles, the alloy was subjected to SEM/EDS analyses. EDS analyses revealed that the black particles were in situ formed alumina particles (Figure 3): they formed due to the reaction of ZrO_2 with aluminum. This can be explained by the fact that, although in the Ellingham diagram (Figure 4), Al_2O_3 and ZrO_2 are quite close to each other with similar free energy of formation over the entire temperature range,

Al_2O_3 is more stable. Hence, at the melting temperature of the alloy, the addition of nanometric ZrO_2 promotes the formation of Al_2O_3 inside the metal matrix.

EDS analyses carried out on small bright phases visible in the alloy microstructure revealed that these are Zr-rich phases (Figure 5). They are formed after the reduction of ZrO_2 to metallic Zr.

To highlight the phases formed in the alloy matrix, an X-ray diffraction was performed. The X-ray diffraction pattern revealed that TiAl, Ti_3Al and Al_2O_3 were the only phases that could be identified. The phase with Zr was too small in quantity ($< 5\%$) to be revealed with this method (Figure 6).
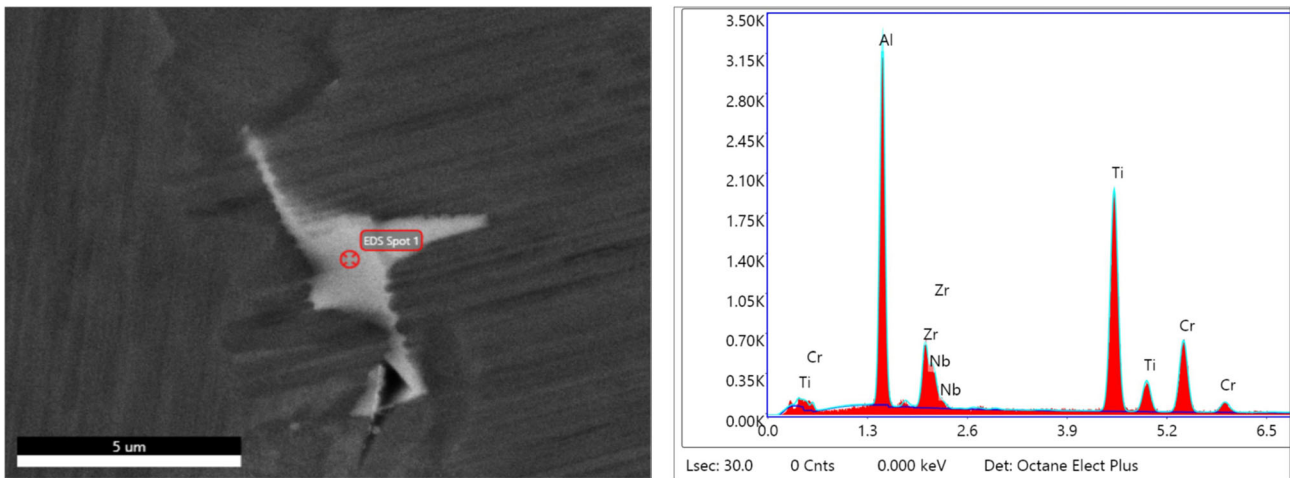

Figure 5. SEM micrograph showing a white phase and EDS spectrum highlighting its composition.
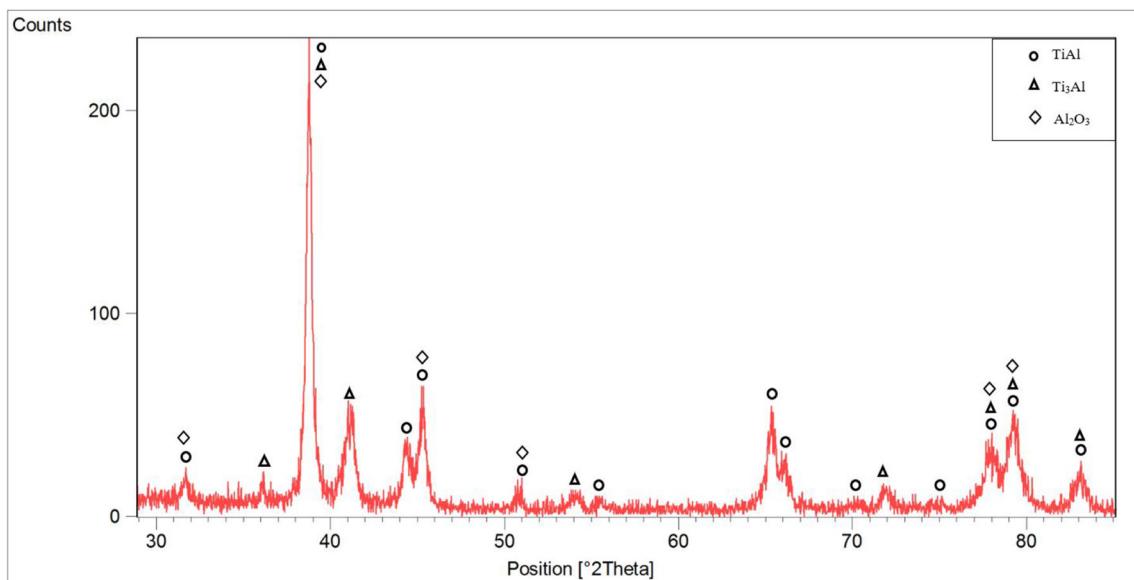

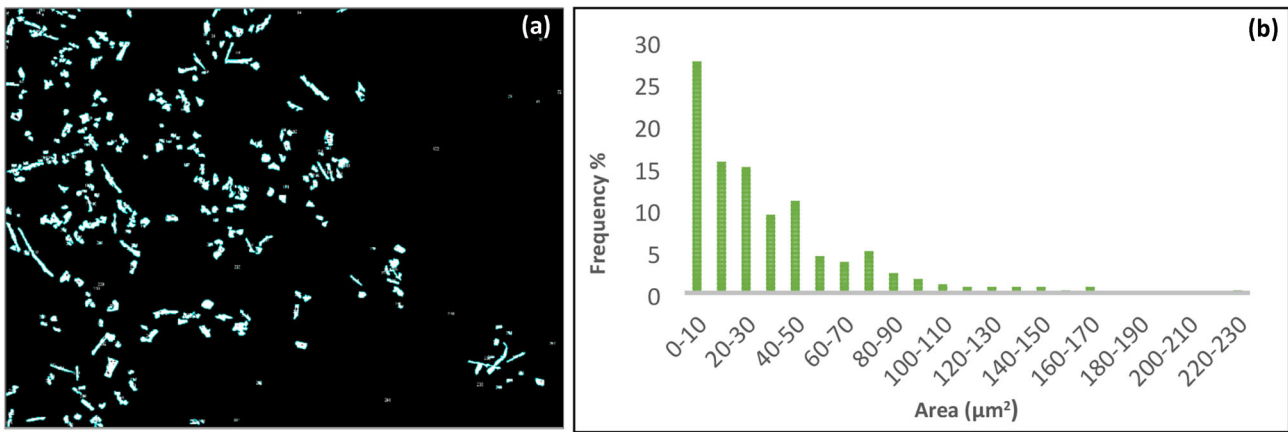**Figure 6. X-ray diffraction pattern of the cast alloy.**

Figure 7. Image analysis of Al$_2$O$_3$ particles (a), showing the particle size distribution in the sample (b).
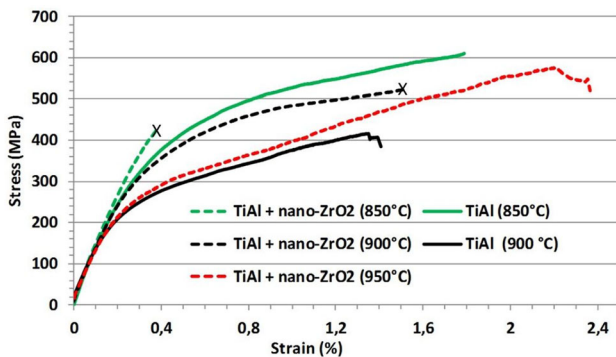

Figure 8. Stress–strain curves obtained from four-point bending test carried out at different temperatures on specimens with and without dispersed particles. The X at the end of the stress–strain curves indicates the fracture.

Figure 9. Elastic modulus vs. temperature obtained from four-point bending tests carried out on the standard and dispersion-strengthened alloy.

SEM micrographs were image analyzed to verify distribution and homogeneity of dispersed alumina particles within the metal matrix (Figure 7). It can be seen that the in situ formed alumina forms aggregated particles well visible in the figure and the image analysis has shown that 78% of them have a size lower than 50 μm^2. The calculated percentage of alumina particles is about 4.15%. Improvements in the particle distribution could be obtained by charging in the crucible well mixed powders, but this is not possible by using our furnace because the induction furnace does not allow to melt powder of reactive metals, which are usually covered by oxides. Preliminary tests showed that remelting the alloy improves the homogeneity of the oxide distribution.

Once the composition was determined for all the castings, the samples were prepared and subjected to bending tests. As already said, the most relevant use of these alloys is for gas turbine blades and rotors, which work at high temperatures; thus, the mechanical bending tests were performed at room temperature and over the temperature range 850–950 °C.
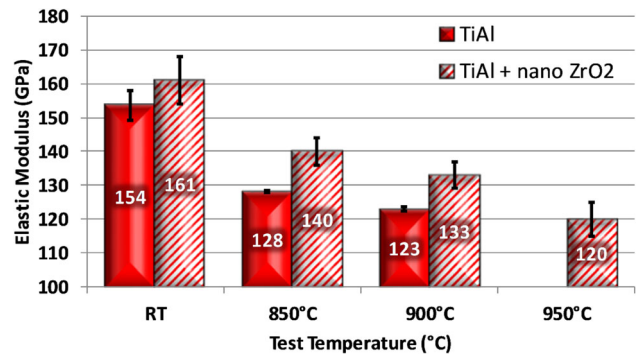
These kinds of experimental intermetallic alloys are generally produced either by hot isostatic pressing or additive manufacturing, so it becomes very important to analyze the effect, at different temperatures, of the dispersion of in situ formed alumina on Young's modulus and yield stress of the cast alloys. The dispersion strengthening is a typical mechanism used for increasing elastic limit, hardness, and creep resistance. The addition of ZrO$_2$, necessary to form in situ Al$_2$O$_3$, was experimented to produce an Al$_2$O$_3$ dispersion that could be very effective in improving the alloy mechanical properties. Figure 8 shows the stress–strain curves of the specimens over the temperature range 850–950 °C. From the curves, it is quite evident that the in situ formed alumina increases the yield stress and Young's modulus over the considered temperature range, which is beneficial in extreme conditions such as gas-turbine applications. It can also be noticed that, at the lowest test temperature, the in situ formed alumina makes the alloy more brittle and sensible to the presence of defects that act as stress intensifiers.

Figure 9 compares the Young's modulus of the in situ reinforced alloy with the one of the base alloy at different

temperatures. This figure clearly shows that alumina formed in situ in the metallic matrix increases Young's modulus at the considered temperatures. The Young's modulus increases by about 5% at room temperature, 10% at 850 °C, 8% at 900 °C. Hence, as the temperature increases, the effect of in situ formed alumina decreases. Figure 10 shows the yield strength as a function of test temperature for both the strengthened and the reference alloy. From the graph (Figure 10), it is evident that there is an interaction between dislocations and oxides with consequent increase of the yield strength at high temperature. This strength increase is ascribable to the Orowan mechanism. At 850 °C, the yield strength increases by 21% and at 900 °C it increases by 35%. At 850 and 900 °C, the reference specimens bent but did not fracture when tested in 4-point bending, while the strengthened alloy fractured both at 850 °C and 900 °C and bent at 950 °C (Figure 11).

By comparing the results obtained in this research with the results obtained in a previous published work,[18] in which we tested a TiAl alloy reinforced with nanometric alumina particles, it is evident that in situ formed alumina allows to obtain better mechanical properties. Yield stress obtained with nanometric alumina dispersion is 372 MPa at 850 °C and 267 MPa at 900 °C, w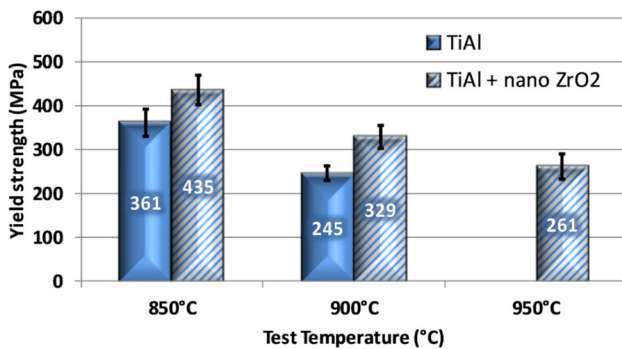hile yield stress obtained with in situ formed alumina reaches 435 MPa at 850 °C and 329 MPa at 900 °C. This comparison highlights also that, by using in situ formed alumina instead of dispersed alumina particles, the Young's Modulus increases from 132 to 140 GPa at 850 °C and from 128 to 133 GPa at 900 °C. The in situ formed alumina allows to improve the mechanical properties because the in situ reaction allows to obtain a higher percentage of small dispersoids (area lower than 10 μm^2) in comparison with those obtained by nanometric alumina dispersion and it allows to improve the interface between the particles and the metallic matrix.

Once the bending test was performed, the fractured specimens were inspected by SEM. SEM analyses highlighted that the fracture propagates through a transgranular path at all the tested temperatures. It should also be said that inside the lamellar colonies the fracture propagates with a mechanism that produces both translamellar and interlamellar fracture. The addition of ZrO_2 has increased the number of shrinkage cavities inside the metal matrix (Figure 11), which favor crack initiation and propagation. This can be explained considering that the samples are thin and that when alumina forms, alumina particles at the microscopic scale, hinder liquid metal flow and thus liquid metal cannot compensate for the alloy shrinkage during solidification. In all of the samples that were produced, there was a larger number of cavities in the alloy compared to those of the samples without dispersion strengthening. Despite the presence of these cavities, the final alloy has better mechanical properties compared to the one without dispersion strengthening. Figure 12 shows the alloy fracture surface at room temperature, which is very brittle and translamellar in nature and propagates through the cavities. By observing Figure 12, it can be noticed that in the presence of alumina, inside the cavities there are polyhedric crystals with sharp edges together with dendrites. The nucleation of these crystals, already noticed in TiAl-based alloys containing dispersed nanometric alumina, is probably favored by the presence of these dispersoids. The fracture at 850 °C (Figure 13) is translamellar with visible secondary cracks and also interlamellar. At 900 °C (Figure 14) again the brittle fracture appears to be both translamellar and interlamellar; moreover, shrinkage cavities are visible on the fracture surface.

Figure 10. Yield strength vs. temperature obtained from four-point bending tests carried out on standard and dispersion-strengthened alloy.

Figure 11. Macrographs showing a shrinkage cavity (left) on a fracture surface and a bent specimen (right) after mechanical test at 950 °C.
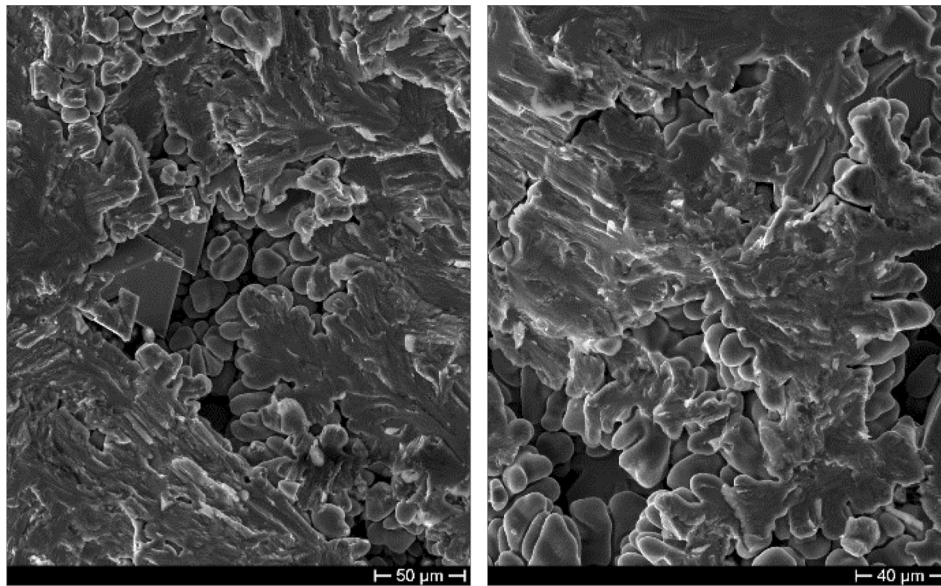
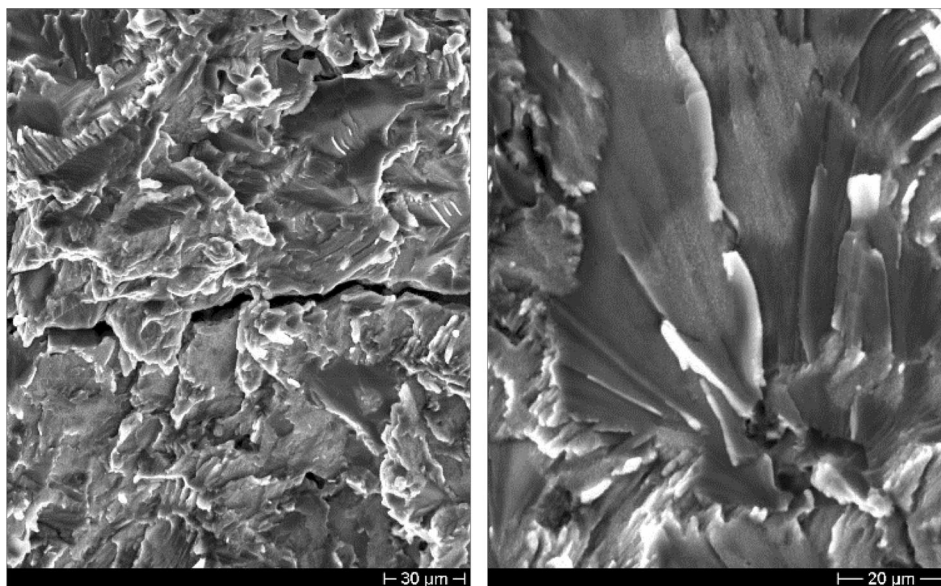**Figure 12. SEM micrographs showing the fracture surface of the dispersion-strengthened alloy tested at room temperature.**

Figure 13. SEM micrographs showing the fracture surface of the dispersion-strengthened alloy tested at 850 °C.

Conclusions

The results reported in this paper highlighted that in situ formed alumina allows to strongly improve the mechanical properties of TiAl alloys at high temperature. By comparing the behavior of the TiAl matrix composite, reinforced with in situ formed alumina, with the behavior of the base TiAl alloy, it has been found that, by using in situ formed alumina, the yield stress increases by 20% at 850 °C and by 34% at 900 °C, while the Young's modulus increases by 9% at 850 °C and by 8% at 900 °C. The improved mechanical performances at high temperature
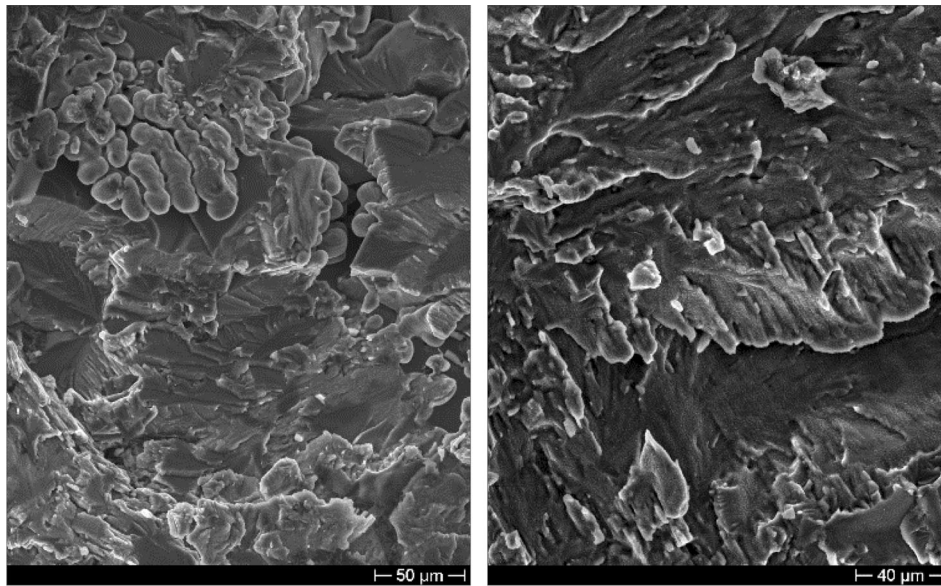
Figure 14. SEM micrographs showing the fracture surface of the dispersion-strengthened alloy tested at 900 °C.

broaden the field of application of these alloys. Further improvements could be obtained by homogenizing the distribution of oxide particles and by designing the gating system to avoid formation of shrinkage cavities.

Conflict of interest The authors have no competing interests to declare that are relevant to the content of this article.

REFERENCES

1. H. Clemens, W. Smarsly, Light-weight intermetallic titanium aluminides—status of research and development. Adv. Mater. Res. **278**, 551–556 (2011). https://doi.org/10.4028/www.scientific.net/AMR.278.551
2. Y.-W. Kim, Gamma titanium aluminides: their status and future. JOM. **47**, 39–42 (1995). https://doi.org/10.1007/BF03221229
3. F. Appel, U. Brossmann, U. Christoph, S. Eggert, P. Janschek, U. Lorenz, J. Müllauer, M. Oehring, J.D.H. Paul, Recent progress in the development of gamma titanium aluminide alloys. Adv. Eng. Mater. **2**, 699–720 (2000). https://doi.org/10.1002/1527-2648(200011)2:11%3c699::AID-ADEM699%3e3.0.CO;2-J
4. H. Clemens, S. Mayer, Intermetallic titanium aluminides in aerospace applications—processing, microstructure and properties. Mater. High Temp. **33**, 560–570 (2016). https://doi.org/10.1080/09603409.2016.1163792
5. B.P. Bewlay, S. Nag, A. Suzuki, M.J. Weimer, TiAl alloys in commercial aircraft engines. Mater. High Temp. **33**, 549–559 (2016). https://doi.org/10.1080/09603409.2016.1183068
6. T. Tetsui, Development of a second generation TiAl turbocharger, Materials Science Forum. 561–565 (Part I), PP. 379–382 (2007). https://doi.org/10.4028/0-87849-462-6.379.
7. T. Noda, Application of cast gamma TiAl for automobiles. Intermetallics (Barking) **6**, 709–713 (1998). https://doi.org/10.1016/s0966-9795(98)00060-0
8. M.M. Keller, P.E. Jones, W.J. Porter, D. Eylon, The development of low-cost TiAl automotive valves. JOM. **49**, 42–44 (1997). https://doi.org/10.1007/BF02914683

9. K. Liu, Y.C. Ma, M. Gao, G.B. Rao, Y.Y. Li, K. Wei, X. Wu, M.H. Loretto, Single step centrifugal casting TiAl automotive valves. Intermetallics (Barking) (2005). https://doi.org/10.1016/j.intermet.2004.12.004

10. Titanium Aluminides and Related Phases, in: Intermetallics (Barking), John Wiley & Sons, Ltd, 1995: pp. 14–38. https://doi.org/10.1002/9783527615414.ch3.

11. J. Fan, Z. Wei, Y. Li, Y. Wang, S. Wu, X. Zhou, J. Liu, J. Guo, Lamellae orientation control and mechanical properties of directionally solidified binary Ti-49Al alloy in oxide ceramics crucible. Int. J. Metalcast. (2021). https://doi.org/10.1007/s40962-021-00614-7

12 R. Feng, W. Song, H. Li, Y. Qi, H. Qiao, L. Li, Effects of annealing on the residual stress in γ-TiAl alloy by molecular dynamics simulation. Materials (2018). https://doi.org/10.3390/ma11061025

13. I. Khaled, Prediction of shrinkage porosity in Ti-46Al-8Nb tilt-casting using the niyama criterion function. Int. J. Metalcast. **7**, 35–42 (2013). https://doi.org/10.1007/BF03355562

14. J. Yang, Y. Wu, R. Hu, Z. Gao, Fabrication and microstructure optimization of TiAl castings using a combined melting/pouring/heat treatment device. Int. J. Metalcast. **15**, 890–898 (2021). https://doi.org/10.1007/s40962-020-00525-z

15. A. Brotzu, F. Felli, D. Pilone, Effects of the manufacturing process on fracture behaviour of cast TiAl intermetallic alloys. Frattura Ed Integrita Strutturale **8**, 66–73 (2014)

16. A. Brotzu, F. Felli, A. Mondal, D. Pilone, Production issues in the manufacturing of TiAl turbine blades by investment casting. Procedia Struct. Integr. (2020). https://doi.org/10.1016/j.prostr.2020.04.012

17 A. Brotzu, F. Felli, F. Marra, D. Pilone, G. Pulci, Mechanical properties of a TiAl-based alloy at room and high temperatures. Mater. Sci. Technol. (United Kingdom) (2018). https://doi.org/10.1080/02670836.2018.1491931

18. D. Pilone, G. Pulci, L. Paglia, A. Mondal, F. Marra, F. Felli, A. Brotzu, Mechanical behaviour of an Al_2O_3 dispersion strengthened γTiAl alloy produced by centrifugal casting. Metals (Basel) **10**, 1457 (2020). https://doi.org/10.3390/met10111457

19. J.S. Benjamin, Dispersion strengthened superalloys by mechanical alloying, metallurgical. Transactions **1**, 2943–2951 (1970). https://doi.org/10.1007/BF03037835

20. K. Zhang, F. Wang, J. Zhu, L. Ye, The microstructures and mechanical properties of V2O 5-Doped Al_2O_3/TiAl in-situ composites by reactive hot pressing process. J. Mater. Eng. Perform. **22**, 3933–3939 (2013). https://doi.org/10.1007/s11665-013-0673-1

21. D. Gu, Z. Wang, Y. Shen, Q. Li, Y. Li, In-situ TiC particle reinforced Ti-Al matrix composites: powder preparation by mechanical alloying and selective laser melting behavior. Appl. Surf. Sci. **255**, 9230–9240 (2009). https://doi.org/10.1016/j.apsusc.2009.07.008

22. X. Liang, Z. Liu, H. Li, F. Chen, W. Yang, S. Ouyang, Y. Liu, L. Wang, Microstructure and elevated-temperature mechanical properties of in situ Ti2AlNb-reinforced TiAl-matrix composite prepared by powder metallurgy. Mater. Today Commun. (2020). https://doi.org/10.1016/j.mtcomm.2020.101179

23. X. Lu, J. Li, X. Chen, J. Qiu, Y. Wang, B. Liu, Y. Liu, M. Rashad, F. Pan, Mechanical, tribological and electrochemical corrosion properties of in-situ synthesized Al_2O_3/TiAl composites. Intermetallics (Barking) (2020). https://doi.org/10.1016/j.intermet.2020.106758

24. L. Xiang, F. Wang, J. Zhu, X. Wang, Mechanical properties and microstructure of Al_2O_3/TiAl in situ composites doped with Cr2O3. Mater. Sci. Eng. A **528**, 3337–3341 (2011). https://doi.org/10.1016/j.msea.2011.01.006

25 L.Y. X, F. W, J.F. Z, X.F. W, Microstructure and mechanical properties of Al_2O_3/TiAl in situ composites doped with Fe_2O_3. Mater. Sci. Forum **675 677**, 597–600 (2011). https://doi.org/10.4028/www.scientific.net/MSF.675-677.597

26. G.L. Adabo, G.R. de Paula, F. Nogueira, L.M.G. Fais, O. Peitl, A quality assessment of titanium castings produced in an experimental short-heating-cycle investment. Mater. Res. **17**, 420–426 (2014). https://doi.org/10.1590/S1516-14392013005000194

27. F. Nogueira, L.M.G. Fais, R.G. Fonseca, G.L. Adabo, The influence of short-heating-cycle investments on the quality of commercially pure titanium castings. J. Prosthet. Dent. **104**, 265–272 (2010). https://doi.org/10.1016/S0022-3913(10)60136-9

28. ASTM International, ASTM C1211-13. Standard test method for flexural strength of advanced ceramics at elevated temperatures, vol 15.01, p. 17 (2013). https://doi.org/10.1520/C1211-13

29. ASTM International, ASTM C1161-13. Standard test method for flexural strength of advanced ceramics at ambient temperatures, vol 15.01, p. 17 (2013). https://doi.org/10.1520/C1161-13

30 O. Kubaschewski, G. V. Samsonov (Ed.): The oxide handbook, 2nd Edition. IFI/Plenum, New York and London 1982. 463 Seiten, Preis: $75,-. Berichte Der Bunsengesellschaft Für Physikalische Chemie **86**, 761–762 (1982). https://doi.org/10.1002/bbpc.19820860820